Resonant exciton contributions to quantum-well electroabsorption

Witold Bardyszewski
Institute of Theoretical Physics, Warsaw University, ul Hoża 69, Warsaw, Poland
and Department of Physics, University of Waterloo, 200 University Avenue West, Waterloo, Ontario N2L 3G1, Canada

David Yevick
Department of Physics, University of Waterloo, 200 University Avenue West, Waterloo, Ontario N2L 3G1, Canada

Claude Rolland and Emmanuel Dupont
Advanced Technology Laboratory, Nortel Networks, P.O. Box 3511, Station C, Ottawa, Ontario K1Y 4H7, Canada
(Received 12 July 1999)

We demonstrate that electroabsorption in shallow multiple quantum-well materials can be significantly affected by the presence of excitons in which the electron or hole occupies a three-dimensional resonant state. The calculated and experimental absorption spectra are seen to retain a two-dimensional character even for photon energies above the quantum well threshold. Additional steplike features that appear in the high energy portion of the absorption spectra, especially at high electric field, are further shown to be associated with the resonant exciton states transitions. Our theoretical results are in excellent agreement with experimental measurements on multiple quantum-well systems with small conduction band energy discontinuities.
[S0163-1829(99)11447-4]

I. INTRODUCTION

The electro-optic spectra of semiconductor quantum wells and superlattices displays many complicated features as a result of exciton formation. Additionally, the applied electric field modifies the one-particle density of states leading to effects such as Wannier-Stark localization in superlattices and field induced tunneling from isolated quantum wells. Models of Stark-ladder transitions associated with Wannier-Stark localization in superlattices formed from strongly coupled quantum wells however generally consider only the lowest miniband originating from the most localized quantum-well level.[1] While a simple tight-binding or transfer matrix calculation of the energy spectra that employs the single lowest superlattice miniband usually yields reasonable results for the electric field dependence of the one-particle states, the results are limited to a narrow spectral range. Moreover, excitonic formation in coupled quantum wells is known to partially inhibit spatially indirect transitions which in turn suppresses Stark-ladder effects.[2] The degree of Stark-ladder features accordingly depends on the relative magnitudes of the exciton binding energy and the superlattice miniband width.

In shallow quantum-well superlattices it is necessary to consider not only the lowest miniband but also higher minibands with energies above the quantum-well threshold. In the presence of the external electric field the latter gives rise to quasilocalized states with wave functions extending over several periods of the superlattice. The field induced localization may then be strong enough to enhance the electron-hole Coulomb coupling leading to the formation of a resonant exciton state. Such a process in fact is observed in the emission spectra in many practical devices such as high frequency and high output power optical modulators based on multiple shallow quantum wells. These materials display numerous features at high-energy that cannot be described by the tight-binding model. The objective of this paper is therefore to present a unified theory that correctly predicts the observed emission.

Section II of the paper determines the local density of states in a finite electric field from a numerical analysis of the MQW problem including the effect of localization and interwell tunneling. The subsequent section extends the standard QW exciton model to include resonant levels in the three-dimensional continuum of states. Finally a comparison is effected between theoretical and experimental results.

II. ELECTRONIC SPECTRUM IN SHALLOW QUANTUM WELLS

Consider a quantum-well material with a small conduction band discontinuity that supports a single bound state in the conduction band and numerous localized heavy hole states. As the exciton transition intensity is proportional to the electron-hole wave-function overlap integral, we first determine the electron energy levels and broadening factors from the local density of states of electrons in the quantum-well region. For this purpose we employ the local density of states defined by the projection

$$A(E)=\int_{QW}|\Phi_E(z)|^2dz \tag{1}$$

onto the well region of $\Phi_E(z)$, the energy dependent solution of the one-dimensional Schrödinger equation for the conduction band electrons in the growth direction normalized to a Dirac delta function with respect to E. The integral in the above definition is taken over the entire quantum-well and barrier region in order to model the localization of the hole and thus the exciton in the quantum well.

 ©1999 The American Physical Society

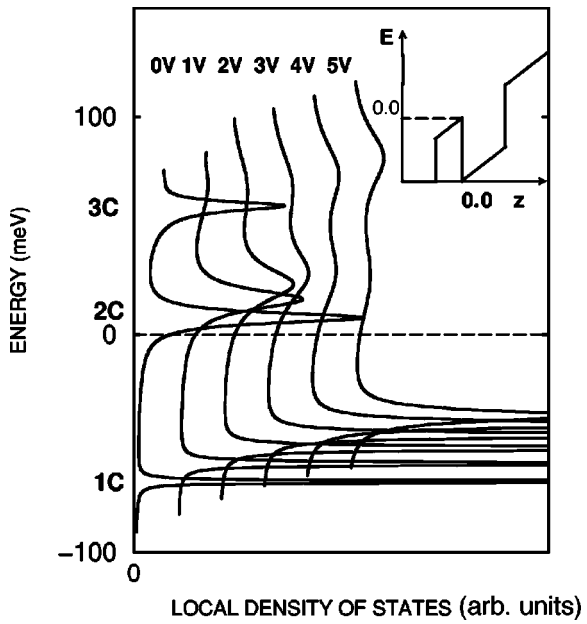

FIG. 1. The evolution of the local density of states for electrons in a single quantum well at applied voltages of 0, 1, 2, 3, 4, and 5 V corresponding to electric fields from 25.5 to 150 kV/cm.

A typical plot of the local density of states with electric field for a single quantum well is presented in Fig. 1. These calculations were performed by applying the finite-difference approximation to the one-dimensional Schrödinger equation for an electron with an effective mass $m_e = 0.0489 m_0$ in the potential shown in the inset which has a conduction band discontinuity of 108 meV, a well width of 95 Å and a barrier width of 80 Å. Vanishing and standing wave boundary conditions for $z \to +\infty$ and $z < 0$ were assumed, respectively. At each field value, three distinctive maxima are present corresponding to the lowest $1C$, $2C$, and $3C$ conduction-band resonant levels. Of these, the $1C$ level energy is lower than the quantum-well threshold E_0, which is taken as the energy reference point in the figure, while the higher two resonances remain in the continuum. As well, the field-dependent shift and broadening of the levels is observed. The general shape of the spectral resonances is, however, preserved up to the largest field shown.

The solution $\Phi_E(z)$ depends in general not only on the potential profile but also on the boundary conditions. Passing to the discussion of multiple quantum-well systems it is instructive to consider at first a solution satisfying the Bloch type boundary condition

$$\Phi(z + L_w) = \Phi(z) e^{ik_z L_w}, \tag{2}$$

where L_w is the sum of the well and barrier widths. These solutions can be thought of as a local miniband structure for each unit cell of length L_w. In a superlattice, an applied electric field misaligns the local allowed bands described by real values of k_z, such that the local forbidden energy gaps of one unit cell with imaginary values of k_z, constitute a barrier for the allowed energy bands of the adjacent quantum well. Thus an enhanced particle localization and therefore decreased resonance width will typically result from multiple reflections and interference.

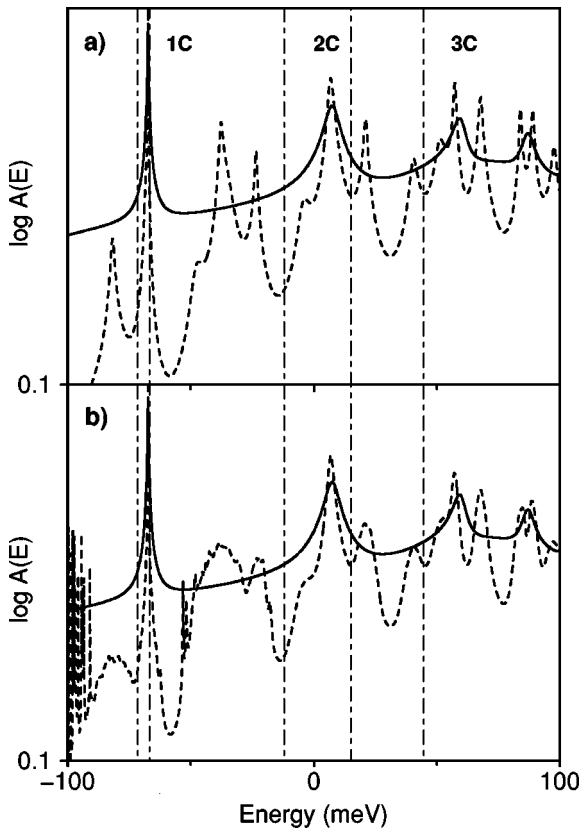

FIG. 2. (a) A comparison of the local density of states of a single quantum well (solid line) and the local density calculated for the system of ten quantum wells and projected onto the quantum-well region with greatest potential (dashed line) for a 25.5 kV/cm applied field. (b) Same as (a) except for the system of ten quantum wells averaged over an ensemble of 100 realizations of MQW systems with random fluctuations of the interface positions from their nominal values given by a normal distribution with a standard deviation of 5 Å. Vertical dash-dotted lines denote the edges of the local energy bands.

The localization enhancement due to interference in multiple quantum-well systems is illustrated in Fig. 2(a) which presents the local density of states of a single quantum well (solid line) for the potential profile given in Fig. 3(a) and for an additional structure obtained by adding nine quantum wells (dashed line) to the low potential side of the original quantum well shown in Fig. 3(b). The energy reference point E_0 is in both cases chosen to correspond to the maximum value attained by the lower barrier of the quantum well in question. The boundary conditions used in this calculation are $\Phi_E(z) \to 0$ for $z \to +\infty$ and $\Phi_E(z) = A \sin(kz + \phi)$ for $z < 0$. The local energy band positions as derived from Eq. (2) are shown in this figure by vertical dashed-dotted lines.

The presence of additional wells clearly narrows the single well resonances without significantly changing their positions. Despite the splitting of the second and third conduction band levels the dominant resonance lines in the MQW system are thus reasonably well represented by the broad resonances of an isolated well. The additional, small intensity resonances in the 10 well system originate from the localized states of neighboring wells that contribute to Eq. (1). Observe also that the position of the lowest energy level of the isolated QW approximately coincides with the upper

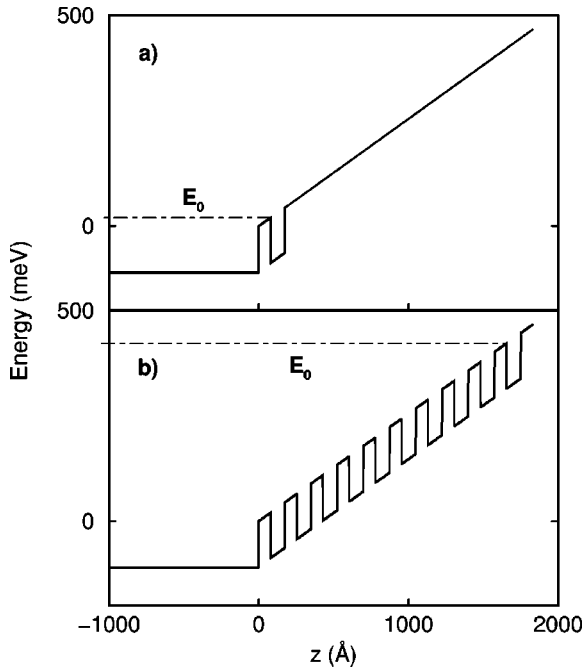

FIG. 3. The potential profile employed in the density of states calculations for (a) a single quantum well and (b) ten quantum wells. The horizontal dash-dotted lines denote the energy reference point (zero of energy) for each potential.

edge of the lowest local energy band of the superlattice. This behavior is equally predicted by a simple tight binding calculation model that employs only the lowest, strongly localized state of the isolated well. On the other hand, the higher energy resonances that branch away from the upper edges of the corresponding energy bands require more sophisticated analysis techniques.

The interference induced localization depends strongly on the coherence length of the electron wave function in realistic systems.[3] Correspondingly, in Fig. 2(b), we explore the effects of small parameter fluctuations of the individual quantum-well in the 10 well system. In particular, to generate a realization of the random potential the position of each interface is changed by a random value Δz that obeys a normal probability distribution with standard deviation $\sigma = 5$ Å and the corresponding density of states is calculated. This process is repeated 100 times and the individual results for the density of states are averaged. The averaged density of states (dashed line) is seen to be nearly identical to that of the isolated quantum well (solid line) since the additional contributions that result from the penetration of the localized states in the adjacent wells largely cancel after averaging. This result indicates that the fluctuations in a real systems caused either by static disorder or thermal oscillations prevent the formation of satellite states over length scales much greater than a superlattice period. Accordingly, we conclude that even for shallow quantum wells the MQW electroabsorption spectra is given by an isolated quantum-well model that includes resonant states. The localization of the associated wave-functions within the well is further sufficiently strong that such resonant excitons should be observable experimentally. Note, however, that although our approximations give the correct level positions, the calculated resonance widths for the single QW case provide only a lower limit for the tunneling escape times.

III. EXCITONS IN THE CONTINUUM

Since in the presence of an electric field no true bound states exist in MQW well systems, a comprehensive analysis must incorporate the entire continuum region of the one-particle states. Unfortunately, the electron-hole Coulomb interaction is difficult to incorporate into such a model. Most theories of excitonic absorption in the quantum-well systems thus consider only the strongly localized states of wells with large potential barriers. The electric field-induced tunneling is then incorporated by applying a uniform broadening to the excitonic lines. In the succeeding calculation, a similar approach will be applied to the resonant levels above the ionization edge in the energy region for which, according to the previous discussion, the local density of states in the energy interval of interest is still dominated by strong resonances.

A full description of the one-particle spectrum for the in-plane momentum $\vec{k}=0$ is contained in the retarded Green's function, which is a solution of

$$[\hat{\mathbf{T}}(\hat{k}_z)+U(z)-E]G(z,z')=\delta(z-z'), \tag{3}$$

where $\hat{\mathbf{T}}$ and $U(z)$ denote the kinetic and potential energy of the electron, respectively. If the continuous spectrum wave functions and energies are Φ_E and E, respectively, $G(z,z')$ has the spectral representation

$$G(z,z')=\int_{E_{\min}}^{+\infty}\frac{\Phi_{E'}(z)\Phi^*_{E'}(z')}{E-E'+i\eta}dE'. \tag{4}$$

In the vicinity of the resonant energy $\tilde{E}_{\rm res}=E_{\rm res}-i\Gamma$ corresponding to outgoing wave solution for $z<z_0$, the Green's function can be approximated by

$$G(z,z')\approx\frac{1}{N}\frac{F_{\rm res}(z)F_{\rm res}(z')}{E-E_{\rm res}+i\Gamma}, \tag{5}$$

where the normalization constant $N=e^{-2\,\mathrm{Im}\,k_0 z_0}\int_{z_0}^{+\infty}|F_{\rm res}(z)|^2dz$ and the complex wave vector k_0 is found from the equation $T(k_0)=E_{\rm res}-i\Gamma$. In accordance with the results of the previous section we approximate the integral over the continuum eigenstates in Eq. (4) by a sum over a small number of resonant states with complex energies $\tilde{E}_{\rm n}=E_{\rm n}-i\Gamma_n$. These states are thus treated as localized bound states that give rise to resonant minibands. The spectrum differs from a discrete spectrum only through the incorporation of the finite resonant state lifetime, which is directly related to the parameter Γ. The Green function then becomes

$$G(z,z')\approx\sum_n\frac{1}{N_n}\frac{F_{{\rm res},n}(z)F_{{\rm res},n}(z')}{E-E_n+i\Gamma_n}. \tag{6}$$

Excitonic wave functions can then be constructed from resonant valence and/or conduction subband states.

To calculate the absorption coefficient according to the method given in the previous publications[4,5] the valence miniband states are represented through the basis set

$$\psi_\nu(\vec{\rho},z)=\frac{1}{\sqrt{A}}F_{m,\mu}(z)e^{i\vec{k}\cdot\vec{\rho}}u_\mu(\vec{\rho},z), \tag{7}$$

where $u_\mu(\vec{\rho},z)$ are the bulk Bloch functions corresponding to the valence band maximum at the Γ point with $k=0$ spin values $\mu=\pm\frac{1}{2}$ and $\mu=\pm\frac{3}{2}$. Each two-dimensional subband can then be given a composite label $\nu=(m,\mu)$ in which $m=1,2,\ldots,$ represents the subband number. The envelope functions $F_{n,\mu}(z)$ for the strongly localized hole levels are evaluated by applying zero boundary conditions at the outer interfaces of both quantum-well barriers. The basis functions are normalized to the unity over the quantum-well area A.

For the resonant conduction subbands we apply

$$\psi_{\mathrm{n}}(\vec{\rho},z)=\frac{1}{\sqrt{A}}F_{res,n}(z)e^{i\vec{k}\cdot\vec{\rho}}u_\nu(\vec{\rho},z), \tag{8}$$

where $u_\nu(\vec{\rho},z)$ is the bulk conduction band wave function at the Γ point for spin values $\nu=\pm\frac{1}{2}$. The envelope function $F_{\mathrm{res},n}(z)$ corresponds to a resonant solution of Eq. (3) with an outgoing wave boundary condition.

Projecting the equation of motion onto the above set of basis functions yields a set of coupled eigenvalue equations for the exciton wave function components associated with all possible electron-hole subband pairs. In this approach, the Coulomb interaction term is explicitly cylindrically symmetric, enabling numerous simplifications. The kinetic energy matrices are generated by projecting the three-dimensional effective mass Hamiltonian onto the above basis function set. In the direct band-gap III-V semiconductor calculations of the following section, a single spherically symmetric conduction band and a light and a heavy hole valence band described by the Luttinger-Kohn Hamiltonian are employed. It is also necessary to include the nonparabolicity in the conduction band to ensure agreement with experiment at large electric fields in our succeeding calculations. Since the valence band of quaternary semiconductors are almost spherically symmetric in the vicinity of the Γ point, a cylindrical approximation can be applied to the effective Hamiltonian for the quantum-well excitons. Exciton eigenstates can then be described in terms of the z projection of the total angular momentum J of the exciton where $J=l+\nu-\mu$ (the negative sign μ stems from the time-reversed nature of the hole states and l represents the z component of the orbital electron-hole pair angular momentum). As a result of the selection rules for excitonic transitions $(l=0,|\nu-\mu|\leqslant 1)$ only the $J=0,\pm 1$ states are optically active.

The quantum-well absorption coefficient is given by the golden rule expression

$$\alpha(\omega)=\frac{4\pi}{cn_r\omega L_w}\sum_J\sum_N|\langle\Psi_N^J|P^J\rangle|^2\mathcal{L}(\omega-E_N^J). \tag{9}$$

Here Ψ_N denotes the Nth solution of the system of coupled exciton equations

$$\sum_{\nu_2}\left[H^X_{0,\nu_1\nu_2}(p)\Psi^J_{N,\nu_2}(p)-\int_0^{+\infty}\frac{dp'}{2\pi}p'U^J_{\nu_1\nu_2}(p,p')\Psi^J_{N,\nu_2}(p')\right]=E_N^J\Psi^J_{N,\nu_1}(p) \tag{10}$$

in which H_0^X and U^J are the kinetic and potential energy part of the electron-hole pair Hamiltonian projected onto the symmetry channel with total angular momentum J. The Coulomb matrix is diagonal with respect to l_ν assuming that the Coulomb interaction is isotropically screened with a dielectric constant ϵ_0. It may be expressed in terms of a single integral over k_z as

$$U^J_{\nu_1\nu_2}(p,p')=\frac{4\pi e^2}{\epsilon_0}\int_{-\infty}^{\infty}\frac{dk_z}{2\pi}\left[\frac{M_{\nu_2\nu_1}(-k_z)M_{cc}(k_z)}{\sqrt{(k_z^2+(p-p')^2)(k_z^2+(p+p')^2)}}\times\left(\frac{\sqrt{(k_z^2+(p+p')^2)}-\sqrt{(k_z^2+(p-p)^2)}}{\sqrt{(k_z^2+(p+p')^2)}+\sqrt{(k_z^2+(p-p')^2)}}\right)^{|l_{\nu_1}|}\right]\delta_{l_{\nu_1}l_{\nu_2}}. \tag{11}$$

In the above equation $M_{\alpha\beta}(k_z)=\int_{-\infty}^{+\infty}dze^{-ik_zz}F_\alpha^*(z)F_\beta(z)$ is the envelope function form factor. Since the Coulomb mixing of the conduction subbands is negligible, the electron is assumed to be in a single specified conduction subband and components of the excitonic wave functions are labeled simply by specifying their valence levels.

Once the excitonic state Ψ_N^J has been determined from Eq. (10), its transition strength is computed from

$$\langle P^J|\Psi_N^J\rangle=\int_0^\infty\frac{dk}{2\pi}k\sum_{\nu_1}P^{J*}_{\nu_1}\Psi^J_{N,\nu_1}(k) \tag{12}$$

in which the momentum matrix element $P^J_{\nu_1}$ for light polarization ϵ is proportional to the overlap of the conduction level c and hole level v envelope functions according to

$$P^J_\nu=M_{c\nu}(0)\frac{1}{V}\int_V d^3x\,u_c^*(\vec{x})\hat{p}_\epsilon u_\nu(\vec{x})\delta_{l_\nu 0}. \tag{13}$$

Note that only the components of P^J with nonzero angular momentum l_ν are nonzero. In addition each excitonic transition is characterized by a specific spectral line shape function $\mathcal{L}(\omega)$.

IV. EXPERIMENTAL PROCEDURE

The physical system considered in this paper consists of a nominally undoped multiple quantum-well structure composed of twenty 95 Å InGaAsP quaternary wells separated by 80 Å barriers grown by metal-organic chemical vapor deposition. The well and barrier widths were precisely determined through TEM measurements. Both wells and barriers are made of a InGaAsP quaternary alloy lattice matched to InP so that, except where specifically noted, all material pa-

rameters employed in the text are obtained by interpolation from binary values. The nominal wavelengths corresponding to the well and barrier energy gaps are $\lambda = 1.48$ μm and $\lambda = 1.1$ μm, respectively, although the value of the energy gap employed in our succeeding calculations is adjusted slightly from these values in order to correctly reproduce the measured absorption edge position at zero applied bias. The associated conduction band discontinuity is then ≈ 100 meV so that even at very weak electric fields only one conduction band level is localized in the well with an energy below the ionization threshold as discussed in Sec. II. All observed heavy hole states on the other hand are strongly localized within each quantum well. The MQW region is finally sandwiched between a *p*-type and an *n*-type InP substrate layer to form a *p-i-n* structure. The built-in voltage of $V_{bi} \approx -1V$ for this diode has been obtained both by fitting the absorption spectra at zero bias voltage and by observing the rapid decrease in quantum efficiency of the diode at $1V$ forward bias.[2]

Measurements of the induced photocurrent spectra were performed on chemically etched, PIN mesa structures with light incident parallel to the growth direction through a window in the top gold contact. To obtain the absolute value of the absorption coefficient, the external bias required to effect a 180° phase change of $\lambda = 1.557$ μm light emerging from a straight 2.2 μm wide, 600 μm long single mode ridge wave guide containing the MQW core and contacted by a metal electrode was measured. The straight wave guide section is placed into one arm of an interferometer as described in Ref. 6 and light polarized parallel to the quantum-well plane is inserted from a tapered fiber into the waveguide through a cleaved and coated end facet. Matching the refractive index change of the MQW material obtained from these measurements excluding the bulk linear electro-optic effect, to the Kramers-Kronig transformation of the electroabsorption spectrum yields the magnitude of the modal absorption arising from the MQW material. The absorption coefficient for the material is then calculated using a theoretical value $\eta = 0.6$ for the overlap factor of the propagating mode overlap factor with the active region. The PIN's and straight wave guides were taken from material produced at the same wafer location in order to ensure a similar material composition.

V. COMPARISON OF THEORY AND EXPERIMENT

To effect a comparison between theory and measurement, we consider a theoretical model incorporating three conduction, two light-hole and six heavy-hole minibands. All input parameters to our numerical program are set empirically as outlined above with the exception of those related to energy level broadening, which enter through the line shape function $\mathcal{L}$ of Eq. (9). To construct this function, we perform an exponential resummation to all powers (cumulant expansion) of the scattering amplitude for exciton-phonon scattering. The resulting $\mathcal{L}$ resembles a Lorentzian for energies less than a LO phonon energy away from its maximum value, but decays nearly exponentially on the lower energy side of the maximum as the energy is decreased away from this region, coinciding with the expected behavior of the Urbach tail.

A second source of broadening is the tunneling out of a given quantum well. This process is modeled according to the procedure outlined in Sec. II. However, Stark localization is only phenomenologically incorporated by limiting the broadening parameter Γ to $\Gamma_{\max} < 10$ meV. The linewidth broadening induced by quantum-well width fluctuations, which are known experimentally to be on the order of $\sigma_W = 5$ Å, varies considerably with resonance energy. To calculate this quantity we therefore calculate the variation of each energy level with well width. This quantity is then used to generate a Gaussian contribution to the linewidth function with a standard deviation deduced from the given value of σ_W. In contrast, local composition fluctuations are assumed to give the same contribution to the linewidth broadening for each resonance and are taken to provide a Gaussian contribution to the line shape with a standard deviation in energy of 12 meV. The Gaussian contribution to the linewidth of each resonance is therefore the square root of the sum over the squared variances of the well width and composition fluctuations. The presence of ionized impurities in the intrinsic region generates a uniform background charge distribution and thus a linear electric field variation across the sample. This effect is modeled with a rectangular contribution to the linewidth. The width of the rectangle is set by the magnitude of the background doping, which is determined here through SIMS measurements. The Urbach type, rectangular and Gaussian contributions are subsequently convoluted to produce the desired linewidth shape function, $\mathcal{L}$.

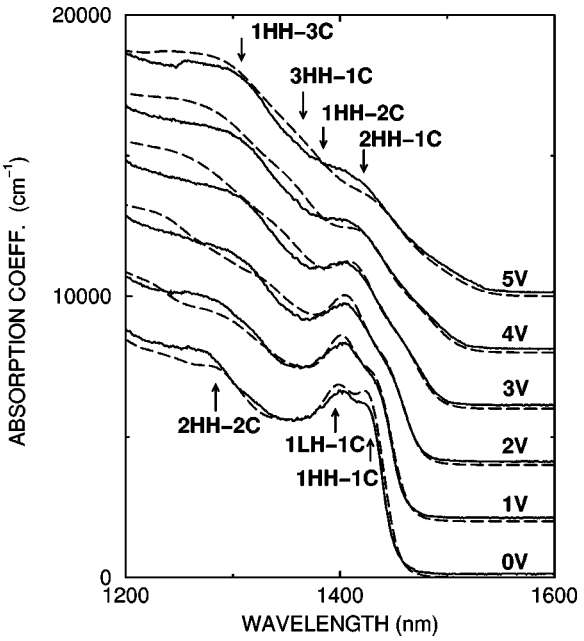

FIG. 4. Experimental (solid lines) and theoretical (dashed lines) room temperature ($T = 300$ K) absorption coefficients for different applied voltages in a PIN diode containing multiple quantum wells.

A comparison between our theoretical curves and the experimental PIN diode measurements for external reverse biases of $U = 0$, 1, 2, 3, 4, and 5 V at a temperature $T = 300$ K is displayed in Fig. 4. Distinct steps in the absorption curve accompanied with additional characteristic two-dimensional excitonic features are observed. In particular a steplike structure at $\lambda = 1300$ nm at $0V$ bias results from the excitonic transition from the second heavy-hole 2HH to the second conduction $2C$ resonant subband. The magnitude of this transition decreases slowly with electric field. At higher field

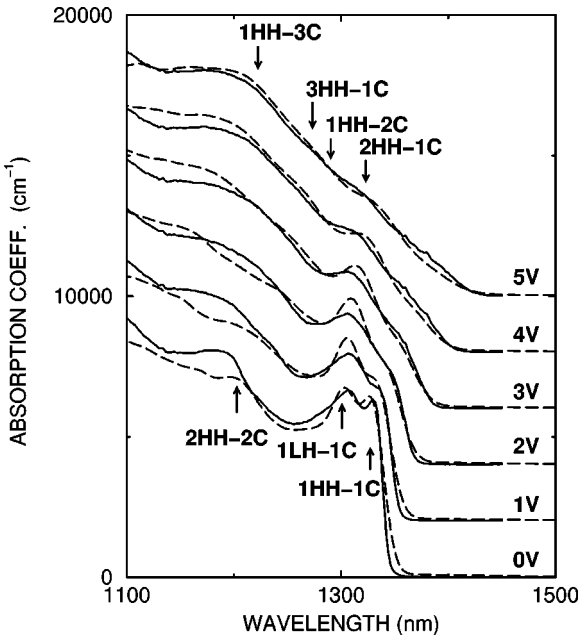

FIG. 5. Same as the previous figure, but for $T=120$ K.

a new step appears in the absorption curve in the vicinity of $\lambda=1300$ nm. This signal, which is most pronounced at $5V$ bias, is associated with the transition from the first heavy-hole to the third, highly resonant conduction subband. The strong broadening at higher applied electric fields obscures the transitions, marked by arrows in Fig. 4, between the third heavy hole 3HH level to the first conduction $1C$ level and the 1HH and the resonant $2C$ level. However, the overall shape of the theoretical absorption spectra that includes the contribution from these two transitions agrees well with experiment.

In order to reduce temperature broadening we repeated the photocurrent measurements on the sample of Fig. 4 at $T=120$ K. Our theoretical results, obtained with the same parameters as in the room temperature calculations, are presented together with the experimental data in Fig. 5. Clearly, the agreement is excellent providing clear evidence for the validity of the linewidth broadening model.

VI. CONCLUSIONS

This paper has discussed several aspects of the theory and behavior of coupled quantum-well materials in an applied electric field. The comprehensive numerical program that was developed to reproduce the low and high energy features of such materials incorporates a cumulant expansion analysis of the resonant excitonic linewidth broadening, the bound and resonant valence and conduction subband structure including the band nonparabolicity and the Coulomb coupling among the various subbands. Our analysis demonstrated that the nonbound resonances that exist in the density of states high above the ionization edge even in relatively shallow quantum wells produce large and predictable steplike excitonic features in the measured electroabsorption that persist at room temperature. The enhanced electro-optic properties associated with such features can be clearly exploited in numerous optoelectronic device applications.

[1] J. Bleuse, G. Bastard, and P. Voisin, Phys. Rev. Lett. **60**, 220 (1988).
[2] A. Fox, D. A. B. Miller, J. E. Cunningham, W. Y. Jan, C. Y. P. Chao, and S. L. Chuang, Phys. Rev. B **46**, 15 365 (1992).
[3] F. Agulló-Rueda, E. Mendez, and J. Hong, Phys. Rev. B **40**, 1357 (1989).
[4] W. Bardyszewski and D. Yevick, Phys. Rev. B **49**, 5368 (1994).
[5] W. Bardyszewski, D. Yevick, Y. Liu, C. Rolland, and S. Bradshaw, J. Appl. Phys. **80**, 1136 (1996).
[6] K. Steijn, R. Leavitt, J. Little, and S. C. Horst, Appl. Phys. Lett. **55**, 383 (1989).